Available online at www.sciencedirect.com
SCIENCE DIRECT®
Biochemical Pharmacology 66 (2003) 663–677
Biochemical Pharmacology
www.elsevier.com/locate/biochempharm

Antidiabetic and antimalarial biguanide drugs are metal-interactive antiproteolytic agents

Deacon Sweeney[a], Michael L. Raymer[a], Thomas D. Lockwood[b,*]

[a]*Department of Computer Science, College of Engineering, Wright State University, Kettering, OH 45429, USA*
[b]*Department of Pharmacology and Toxicology, School of Medicine, Wright State University-Cox BLDG 3525 Southern Blvd, Kettering, OH 45429, USA*

Received 1 October 2002; accepted 25 April 2003

Abstract

Various biguanide derivatives are used as antihyperglycemic and antimalarial drugs (e.g., 1,1-dimethyl biguanide (metformin), phenylethyl biguanide (phenformin), *N*-(4-chlorophenyl)-*N*′-(isopropyl)-imidodicarbonimidic diamide (proguanil)); however, no common mechanism has been suggested in these controversial therapeutic actions. Biguanides bind endogenous metals that inhibit cysteine proteases independently, e.g., Zn^{2+}, Cu^{2+}, Fe^{3+}. Here, various biguanide derivatives are reported to be metal-interactive inhibitors of cathepsin B from mammals and falcipain-2 from *Plasmodium falciparum*. Structural homologies were identified among the Phe-Arg protease substrate motif and the metal complexes of phenformin and proguanil. Molecular modeling revealed that the position of the scissile amide substrate bond corresponds to the biguanide-complexed inhibitory metal when the phenyl groups are homologously aligned. Binding of the phenformin–metal complex within the active site of human cathepsin B was modeled with computational docking. A major binding mode involved binding of the drug phenyl group at the protease S2 subsite, and the complexed inhibitory metal shared between the drug and the protease Cys29-His199 catalytic pair. Cysteine protease inhibition was assayed with carbobenzyloxy-PHE-ARG-7-aminomethylcoumarin substrate. In the absence of metal ions, phenformin was a weakly competitive protease inhibitor (apparent K_i several μM); however, metformin was noninhibitory. In contrast, the metal complexes of both metformin and phenformin were protease inhibitors with potency at therapeutic concentrations. Biguanide–metal complexes were more potent cysteine protease inhibitors than either the biguanide or metal ions alone, i.e., synergistic. Similar to chloroquine, therapeutic extracellular concentrations of metformin, phenformin, and proguanil caused metal-interactive inhibition of lysosomal protein degradation as bioassayed in primary tissue using perfused myocardium. The biguanide moiety is identified as a past and future structural scaffold for synthesis of many protease inhibitors. Results are discussed in relation to Zn^{2+}-interactive inhibition of insulin degradation in hormone target tissues, and Fe^{3+}-interactive inhibition of hemoglobin degradation in parasite food vacuoles. Previous studies on insulin hypercatabolism and insulin resistance are speculatively reviewed in light of present findings.

Keywords: Phenformin; Proguanil; Metformin; Cathepsin B; Falcipain-2; Protease inhibitors; Chloroquine; Intracellular protein degradation; Perfused heart

1. Introduction

Many drugs have been discovered without understanding of their therapeutic targets or chemical determinants. More than 150 derivatives of guanidyl guanidine have been synthesized over 70 years; and a vast number are conceivable [1,2]. Biguanide derivatives are widely used against malaria and type 2 diabetes; however, no mechanistic similarities against these different diseases have been proposed. Retrospective pharmacology seeks to identify structural features, chemical reactivity, and biologic targets of an individual drug with multiple actions or diverse drugs with a common action.

Ongoing drug administration has historically led to discovery of unanticipated secondary actions and their exploitation. The biguanide drug, proguanil, was discovered as

* Corresponding author. Tel.: +1-937-298-3399x54741; fax: +1-937-395-8387.
E-mail address: thomas.lockwood@wright.edu (T.D. Lockwood).

Abbreviations: BAA, *N*-alpha-benzoyl-L-argininamide; Metformin, 1,1-dimethyl biguanide; Phenformin, phenylethyl biguanide; Proguanil, *N*-(4-chlorophenyl)-*N*′-(isopropyl)-imidodicarbonimidic diamide; Z-Phe-Arg-AMC, carbobenzyloxy-L-phenylalanylargininyl-7-amino-methylcoumarin.

0006-2952/$ – see front matter © 2003 Elsevier Inc. All rights reserved.
doi:10.1016/S0006-2952(03)00338-1

an antimalarial agent in the 1940s. Proguanil antimalarial action was attributed solely to the inhibition of parasite dihydrofolate reductase by the metabolite cycloguanil. However, a seemingly unrelated antihyperglycemic side effect of proguanil was noted ([1], and other chapters in this monograph, [2]). The antihyperglycemic effect of proguanil led to subsequent development of other anti (type 2) diabetic biguanide derivatives, including phenformin (phenylethyl biguanide), buformin (*n*-butyl biguanide), and metformin (dimethyl biguanide). Among these antihyperglycemic drugs, metformin is currently used due to its favorable efficacy/toxicity ratio. Neither the parent drug, proguanil, nor the antidiabetic biguanides are known to inhibit dihydrofolate reductase. Conversely, inhibition of dihydrofolate reductase does not exert an antihyperglycemic effect. Multiple biguanide antihyperglycemic mechanisms have been proposed; however, biguanides are not insulin secretagogues. Recent evidence suggests inhibition of the mitochondrial respiratory complex among metformin actions [3,4]. The antimalarial mechanisms of proguanil have also become controversial. It has been reported that the antimalarial actions of proguanil cannot be attributed solely to the antifolate action of its metabolite [5,6]. Additional antimalarial mechanisms of proguanil action have been proposed, including mitochondrial actions [3,4].

An unappreciated relationship in the history of antimalarial and antihyperglycemic drug discovery suggests common therapeutic mechanisms in both diseases. Curiously similar to biguanides, the discovery of chloroquine as an antimalarial drug was followed by discovery of its antidiabetic side effects on both carbohydrate and lipid metabolism [7–20]. The antidiabetic efficacy of chloroquine has led to continuing investigations of its therapeutic use against insulin resistance [11,15,17,20], although toxic risk is appreciable [21,22].

These puzzling observations among two seemingly unrelated drug types and two unrelated diseases, might be readily explained if both chloroquine and biguanide actions include antiproteolytic effects in parasites and human insulin target tissues. Plasmodial growth can be limited by the rate of degradation of host hemoglobin [23–27]. Chloroquine inhibits the vacuolar transporter and protein degradation in parasite lysosomes [28]. Nonspecific cysteine protease inhibitors can also permit host immunity to clear mouse malaria [24]. Thus, known antimalarial drug actions include two distinct antiproteolytic mechanisms mediated by interference with lysosomal acidification, and direct protease inhibition. The duration of insulin action is primarily determined by target tissue degradation of hormone and/or the hormone–receptor complex, independent of additional factors influencing insulin sensitivity [7]. The action of chloroquine has been correlated with inhibition of insulin degradation, and prolongation of hormone actions [7]. Among multiple mechanisms of type 2 diabetes, insulin hypercatabolism is an old concept with recent support ([29,30], see discussion). Protease inhibitors in the treatment of type 2 diabetes are virtually uninvestigated.

Mammalian cathepsin B and plasmodial falcipain are among major proteases contributing to the degradation of insulin and host hemoglobin [23,25,31–34]. These and other cysteine proteases are partially inhibited by endogenous metal ions. Zn^{2+} and Fe^{3+} are natural inhibitors of insulin and hemoglobin degradation, respectively. Upon drug administration the biguanide moiety forms metal complexes in proportion to the relative binding affinities and tissue availabilities of endogenous metals [1]. This background led to the present hypotheses that: (1) Antimalarial and antidiabetic biguanides are unrecognized cysteine protease inhibitors, revealing protease inhibition as a contributing therapeutic mechanism in both diseases. (2) Some biguanide derivatives might co-bind metals and substrate recognition sites so as to enhance the natural inhibitory action of endogenous metals against protease catalytic sites. (3) Fifty years of biguanide use provides a retrospective human laboratory demonstrating feasibility of therapeutic cysteine protease inhibitors *with certain properties*. (4) The biguanide moiety has been, and will be a scaffold for synthesis of protease inhibitors with a wide range of properties. The implied question of insulin hypercatabolism in pathophysiology of insulin resistance is speculatively reviewed.

2. Methods

2.1. Protease assay

Purified protease activities were assayed fluorimetrically by standard methods using carbobenzyloxy-L-phenylalanylargininyl-7-amino-methylcoumarin (Z-Phe-Arg-AMC) as substrate (Bachem), 20 μM, or as described below, 50 mM acetate buffer, 2 mM DTT, pH 5.5. Reaction progress was measured using a microwell plate reader (Lab Systems) equipped with the delta-soft kinetic program that statistically fits the measured initial reaction rate to a linear range ($R > 0.96$). In order to remove trace amounts of contaminating metals proteases were purified with EDTA chelator. Proteases were fully reduced by prior incubation for 10 min in DTT (5 mM). Inhibitors were added to protease-buffer-DTT followed by initiation of reaction with substrate addition, or in the order described in figure legends. Present inhibitor concentrations are far in excess of enzyme active site concentrations. Measured quench of fluorescence was inconsequential at present concentrations of all agents. The apparent inhibitory constants (K_i, app) were characterized using standard methods (reviewed in Ref. [35]). In determination of K_i, app, the control and inhibited reaction rates were essentially linear over the measurement period; and less than 5% of the substrate was depleted.

2.2. Docking of biguanide–metal complex to the active site of cathepsin B

Present studies employ dock modeling to qualitatively compare the predicted fit of a drug ligand within a protease active site with known dimensions of fit of a homologous substrate. The three-dimensional crystal structure of human cathepsin B [36], was obtained from the Protein Data Bank for docking with drug ligands (Figs. 1–3). The active site cysteine-29 was deprotonated to thiolate anion; and the active site histidine-198 was protonated at the epsilon nitrogen to imidazolium cation. These ionizations of the catalytic amino acids are consistent with their known status at the moderately acid pH optimum of the reaction, relative to their p*K*s. Computations of the structures of biguanide–metal complexes employed SYBYL (Tripos Software). The molecular docking program, Hex version 3, was employed to compute sterically and electrostatically feasible enzyme–ligand interactions (reviewed in Refs. [37,38]). Present studies do not attempt a rigorous prediction of protein–ligand binding energies under biologic conditions. Here, dock modeling is limited to display of dimensional feasibility of predicted fit of a drug–metal complex shared between the catalytic pair and substrate-binding subsites of a model cysteine protease [36].

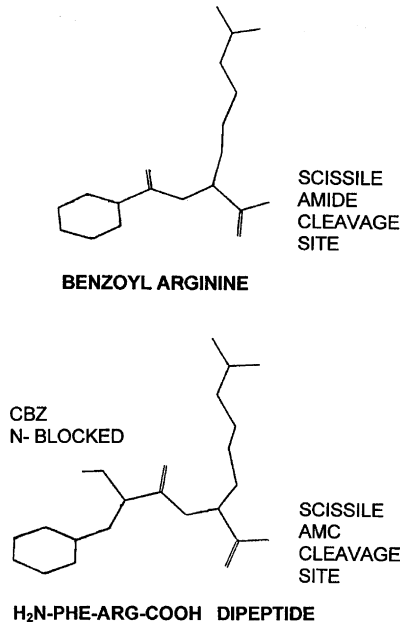

Fig. 1. Structures of benzoyl arginine and phenylalanyl–arginine dipeptide. Computed structures were directed to arbitrary homologous conformations by bond rotations. The difference in distances between phenyl groups and scissile bonds can be accommodated by the dimensions of the S2 substrate-binding pocket shown in Fig. 3. Slight bond rotations can create greater positional homology among the phenyl and guanide groups and the scissile bonds.

2.3. Primary tissue bioassay of subcomponents of cell protein degradation using perfused rat heart

Small hearts from young 160–180 g rats were perfused as Langendorf preparations as previously described [31–33]. A constant flow rate of 7 mL/min provided a constant low perfusion pressure of approximately 40 mmHg. The nonrecirculating perfusate contained Krebs salts, physiologic concentrations of complete amino acids, citrate, pyruvate, lactate, 10 mM glucose, and 0.3% BSA (95% oxygen, 5% carbon dioxide). The pH was monitored continuously. Perfusate was filtered in line. These conditions provide good contractile function for more than 6 hr; however this preparations is not stable under some other conditions routinely employed.

Hearts were biosynthetically labeled with [4,5] [^{3}H]leucine for 15 min prior to addition of nonradioactive leucine to the perfusate (routinely 0.4 mM). The release of trichloroacetic acid soluble radiolabel was measured at 2 min intervals by collection of the total nonrecirculating effluent perfusate with a fraction collector. In order to calculate the percent inhibition of [^{3}H]leucine release each heart is employed as its own internal control. The statistically fitted curvilinear baselines of [^{3}H]leucine release 45 min prior to inhibition were accurately extrapolated over the following periods of inhibition as verified in uninhibited controls. Zero time corresponds to 3 hr after isolation and protein labeling as described below. Results are shown ±SD, N = 3 or more determinations.

Unless reincorporation is prevented, experimental increase in protein synthesis can divert a fraction of radiolabeled postcursor from extracellular release to reincorporation. Following radiolabelling without extracellular leucine, postcursor reincorporation can be prevented either by competitive inhibition with nonradioactive perfusate leucine chase, or elimination of protein synthesis with cycloheximide under physiologic leucine [32]. In the present preparation, these two different methods provided identical conclusions over 1 hr exposures. However, cycloheximide proved toxic after 1 hr, and could not be routinely employed. Following biosynthetic labeling with trace leucine concentration, addition of physiologic 0.1 mM perfusate chase leucine suffices to cause at least 95% maximal external release of radiolabeled postcursor. Fully maximal postcursor release was provided by a chase leucine concentration of 0.2 mM, which is within the upper physiologic range. The percentages of total proteolysis mediated by the lysosomal vs. extralysosomal pathways are defined by various inhibitory agents described below. In order to determine any possible artifact of leucine concentration, the effects of chloroquine and diamide on major proteolytic pathways were compared under the four conditions of physiologic 0.1 mM leucine vs. 1.0 mM leucine, each with and without cycloheximide. As shown below, the percent inhibitions of proteolysis due to chloroquine and diamide were indistinguishable under physiologic leucine (0.1 mM) and supraphysiologic leucine (1.0 mM) (insignificantly different, $P > 0.1$). The

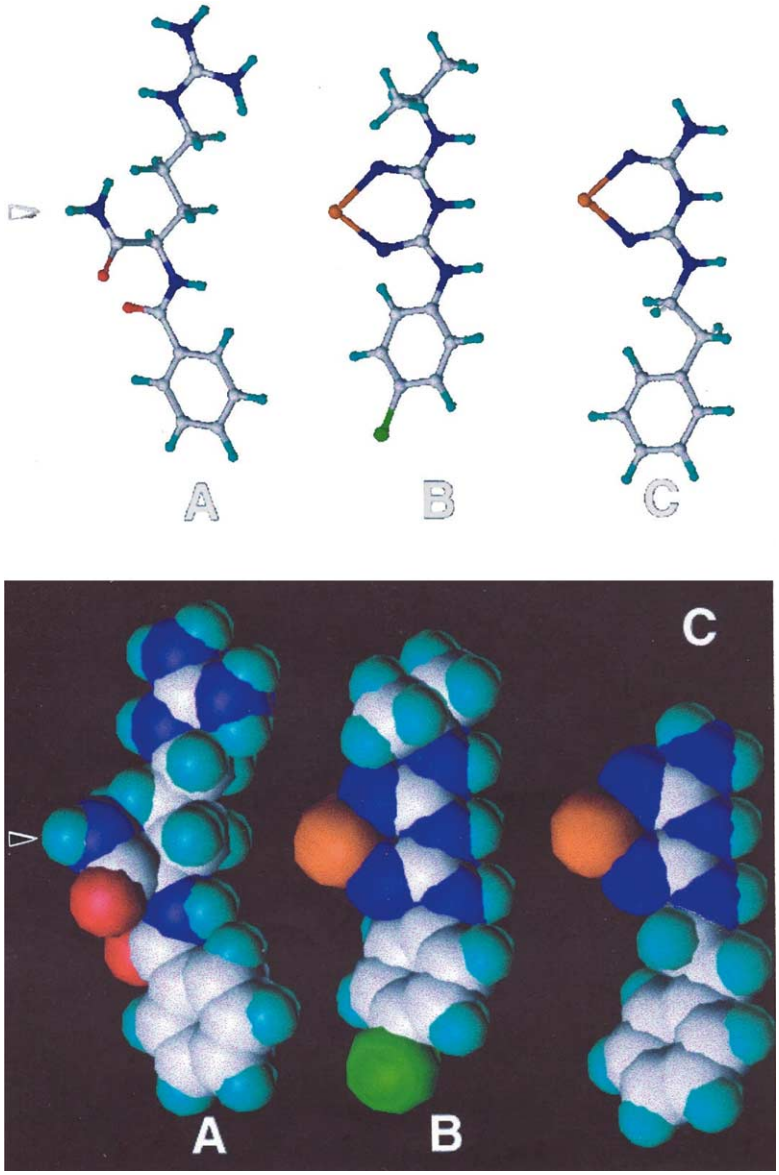

Fig. 2. (A) Benzoyl arginine amide, (B) proguanil–metal complex, and (C) phenformin–metal complex. The biguanide–metal complexes were computed with Fe^{3+}. All conformations are shown as computed at minimal energy. The arrow (left) indicates the scissile amide group of benzoyl arginine amide, which is cleaved by cysteine proteases in use as an artificial substrate. In this illustration the positions of the biguanide-complexed metal ions were aligned horizontally with the position of the scissile amide bond of the synthetic protease substrate. Bond rotations can improve structural homologies (see text). Black: carbon; blue: nitrogen; green: chlorine; red: oxygen; orange: iron.

indicated actions of chloroquine and diamide were also indistinguishable when cycloheximide (20 uM) was included with 0.1 or 1.0 mM leucine over periods of less than 1 hr (data not shown).

2.4. Materials

Native bovine spleen cathepsin B was obtained from Sigma-Aldrich. Recombinant falcipain-2 of *Plasmodium falciparum* was generously provided by the authors of Ref. [29], in which the enzyme is described. The Jacobus Pharmaceutical Company generously provided proguanil. Other drugs were from Sigma-Aldrich. Materials and apparatus for heart perfusion have been previously described [31,32]. Animal care and use was in accord with accepted standards, under institutional review.

3. Results

3.1. Structural and chemical homologies among an antimalarial biguanide, an antidiabetic biguanide, a synthetic protease substrate motif, and peptide cleavage sites preferred by proteases

A cysteine protease can be inhibited by competition against the binding of substrate peptides to protease recognition subsites (associative inhibition) or chemical reac-

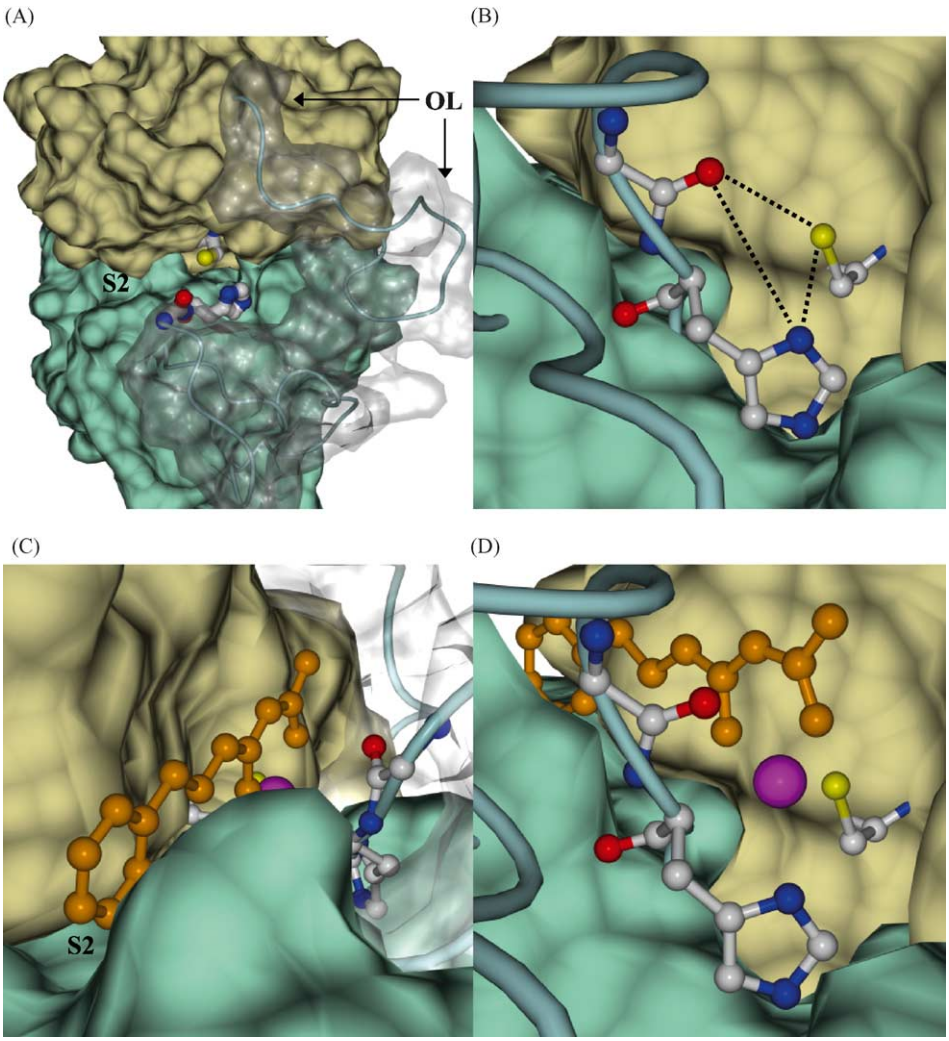

Fig. 3. Docking of Fe^{3+}–phenformin complex within the active site of human cathepsin B. Four different views of the cathepsin B crystal structure are shown [36]. (A, top left) The two lobes of human cathepsin (B) (green and gold) are separated by a central cleft. In all panels, replacement of the peptide backbone with the tube structure artificially smoothes the bond angles of the backbone without otherwise changing structure. Active site amino acids are superimposed upon the smoothed tube structures in positions identical to the reported crystal structure. A segment of the backbone structure referred to as the occluding loop (residues 108–125) partially obstructs the active site (labeled approximately as OL). The opaque surface structure has been partially replaced with translucency in order to permit visualization of the active site within the cleft. The locations of protease S1 and S2′ subsites (not labeled) relative to the S2-binding pocket (labeled) and catalytic pair are described in Refs. [39,40], and the text. Grey: carbon; blue: nitrogen; yellow: sulfur; red: oxygen (B, top right). The vicinal Cys29 thiolate and His199 imidazolium of the catalytic pair are located on separate lobes, separated by the cleft, as shown in ball and stick representation (see Section 2). Also shown are the backbone carbonyl oxygens of Gly198 and His199. The cysteine-29 thiolate sulfur–His199 imidazolium nitrogen–Gly198 carbonyl oxygen triad form a metal-binding site as described in the text (dashed traces). In view A the carbonyl backbone oxygen of His199 can be viewed as below the surface plane of the triangle shown in view B. The distance between the His199 carbonyl oxygen and metal is seemingly greater than that which would contribute appreciably to metal attraction at a location above the plane of the triad (see text) (C, bottom left). The phenyl group of the drug is bound within the S2 subsite pocket (phenformin colored here uniformly amber, see Fig. 2 for coded structure). The coordination of the metal ion shared between the drug biguanide moiety and protease catalytic site is not readily seen in this view. (D) This different view of the same binding mode as in view C shows the position of the Fe^{3+} ion shared between the drug biguanide group and the metal-binding triad described in view B and the text. Inhibitory metal ions alone can bind to the indicated catalytic site without the drug.

tivity with the distinct catalytic pair (reactive inhibition) or both.

3.1.1. Pharmacologic analogues of preferred protease cleavage sites

The PHE-ARG sequence is a preferred cleavage site for cathepsin B and other proteases. Protease catalytic mechanisms are not specific for the peptide bond, but can also mediate hydrolysis of ester or amide bonds in artificial substrates. Among the first synthetic protease substrate motifs, BAA was intuitively designed to be structurally mimetic of Phe-Arg (Fig. 1). Cathepsin B can cleave the scissile amide bond at the carboxyl group of BAA. Carboxyl terminal derivatives of benzoyl arginine, and N-blocked Phe-Arg dipeptide are now widely used in the sensitive assay of protease activity, e.g., Z-Phe-Arg-AMC. The carbobenzyloxy N-blocking group of the dipeptide serves to inhibit amino-exopeptidase action.

The guanidyl guanidine moiety is a metal cation-binding site in association with two lone pairs of nitrogen electrons in close proximity (Fig. 2). The biguanide moiety is known to bind more than 15 cations, including all endogenous metals that can independently inhibit cysteine proteases [1].

Phenformin and proguanil exhibited partial homologies to each other, and the Phe-Arg substrate motif as suggested by the above medical hypotheses, and confirmed by computed structures (Figs. 1 and 2). The hydrophobic character of a phenyl group is vicinal to the biguanide metal-binding sites of the drugs, or the homologous location of the scissile substrate bond. In proguanil the chlorine ring substituent extends the margin of the hydrophobic moiety to a distance approximating dimensional similarity to phenformin. All structures are shown in Fig. 2 as computed in minimal energy conformations without directed bond rotations. Free rotation about the unrestrained peptide bond can provide an infinite continuum of substrate conformations. A substrate peptide might be partitioned among conformations that are structurally homologous to inhibitors, and other conformations that are nonhomologous. Accordingly, a nonhydrolyzable, peptide-mimetic agent might compete against protease binding of some substrate peptide conformations but perhaps not others (see below).

3.1.2. Cysteine protease catalytic sites and reactive inhibitions

The ancestral papain domain of cysteine proteases consists of a single peptide chain folded into two lobes (Fig. 3, green and gold) separated by a central cleft [34,36]. The active site is located within the groove formed by the cleft between the two lobes. The two catalytic amino acids are located on separate lobes, but closely aligned in the three-dimensional structure of the active site. The namesake of cysteine proteases is an active site cysteine that serves to attack the carbonyl carbon of the scissile peptide bond. A histidine group is folded to a position vicinal to the catalytic cysteine. The peptidolytic mechanism involves the ionized thiolate–imidazolium catalytic pair. The moderately acid pH optimum of the reaction mechanism results from the optimal ionization of these acidic and basic amino acids, relative to their respective p*K*s. The catalytic pair invites two types of inactivating reactions, which are independent of remote substrate–inhibitor binding interactions. The Cys-His catalytic pair is a strong metal-binding site; and catalysis can be subverted by endogenous inhibitory metal ions. Second, the active site cysteine can readily oxidize to an inactive form by several reversible reactions of sulfur. Accordingly, routine assay of maximal activity requires reductive activator, such as DTT, and prior metal chelation.

3.1.3. Cysteine protease substrate recognition sites and associative inhibitions

Multiple substrate-binding sites are spatially distinct from the catalytic amino acid pair cleaving the scissile bond [34,39,40]. Substrate recognition sites do not participate directly in excitation or stabilization of a transition state, but rather serve to kinetically enhance substrate bond alignment with the catalytic amino acids. Substrate amino acid sequences flanking the scissile peptide bond (asterisk) are customarily designated: $H2N\cdots P3-P2-P1*P1'-P2'-P3'\cdots COOH$. Substrate-binding subsites of proteases are designated as $S3-S2-S1*S1'-S2'-S3'$, corresponding to the linear sequence of substrate amino acid positions. However, in cathepsin B there is little or no specific relationship between three-dimensional protease subsite structures and the recognition of linear substrate amino acid sequences [39,40]. Each individual cathepsin B subsite can accept multiple substrate amino acids; therefore, protease binding of a polypeptide substrate is the net result of multiple S–P binding interactions. The binding of a substrate amino acid at one subsite can be ''overruled'' by higher affinity binding of others at distinct subsites. In addition, each substrate polypeptide can assume an infinite continuum of conformations, introducing additional complexity to the partition of binding interactions. Some peptide structures can register in multiple subsite alignments. Cathepsin B exhibits macromolecular endoproteolytic cleavage patterns revealing acceptance of a broad array of substrate amino acid sequences and binding alignments. Consistent with broad substrate acceptance, nonhydrolyzable inhibitor structures can also be bound in multiple orientations [41]. Accordingly, competition between an inhibitory ligand and a peptide substrate can involve many interactions with this nonspecific protease active site.

Despite all uncertainties, the P2–S2 interaction is verified as the most important determinate of substrate–cathepsin B interaction [36,39,40]. The S2 subsite is the only site representing a truly recessed binding pocket in the surface of the protease (labeled in Fig. 3). Cathepsin B prefers substrates with bulky hydrophobic amino acids at the P2 position, with greatest preference for phenylalanine. The phenylalanine of the Z-Phe-Arg-AMC substrate of Fig. 1A corresponds to the P2 position of preferred protease substrates. Phenylalanine binding in the recessed S2 pocket is presumably enhanced by hydrophobic interactions. In Fig. 3A, the S1 subsite is located above the labeled S2 subsite, at the left of the catalytic pair, and the S2′ subsite is located on the right of the catalytic pair as reviewed in Refs. [39,40], but not shown here.

3.1.4. Biguanide–metal complexation and recruitment of endogenous inhibitory metals to protease co-binding

When the scissile amide bonds of benzoyl arginine amide or the dipeptide derivative are graphically aligned with the location of the complexed metal of phenformin or proguanil, the positions of hydrophobic ring structures and biguanide moieties correspond (Fig. 2). A homologous orientation of these agents bound within the active site of a cysteine protease would introduce the complexed

inhibitory metal ion to the location of the scissile amide substrate bond cleaved by the enzyme catalytic pair. Accordingly, biguanide–metal–protease co-binding might enhance effective interactions of naturally inhibitory metals with the protease catalytic pair.

3.2. Weak biguanide inhibition of cysteine protease activities in the absence of metal ions

Therapeutic extracellular phenformin concentrations are near 1 μM although not precisely characterized [1]. Targeted metformin concentration range is 15–20 μM although more can be tolerated [21]. Biguanides bind endogenous Zn^{2+}, Cu^{2+}, and Fe^{3+} and other ions with dissociation constants considerably less than 10 exp –6. Accessible intracellular protease inhibitory cation concentrations are present in large excess above drug concentrations. Therefore, at therapeutic phenformin concentration near 1 μM, the estimated free concentration of noncomplexed drug is less than 10 exp −9, i.e., a fraction of less than 1/1000 of the complexed drug. The protease inhibitory action of 10 exp −9 to 10 exp −7 M noncomplexed phenformin is negligible (Fig. 4). Therefore, noncomplexed therapeutic drug actions are inconsequential to therapeutic actions.

Although beyond the present scope, phenformin inhibition of cathepsin B activity toward Z-Phe-Arg-AMC deviated from ideal enzyme kinetics at supratherapeutic concentrations. Under conditions of Fig. 4, metal-free phenformin maximally inhibited approximately 70% of the hydrolysis of Z-Phe-Arg-AMC (5 μM). However, 30% of this activity was not inhibited even under very high concentrations of 100 μM. These multi-component inhibitory properties of phenformin are consistent with the multiple enzyme–substrate/enzyme–inhibitor interactions discussed above. Phenformin concentrations that partially inhibited 5 μM Z-Phe-Arg-AMC hydrolysis had no effect on higher 50 μM substrate concentrations (Fig. 4); therefore, the partial inhibitory effect of free phenformin is competitive relative to this substrate. Figure 4 illustrates technical obstacles to characterization of free phenformin protease inhibition using customary enzyme kinetics. Determination of the inhibitory constant, K_i app, would include the average of inhibitable and noninhibitable subcomponents. Inhibition of the sensitive subcomponent can be estimated by subtraction of the uninhibitable subcomponent, although the interpretation is uncertain. Using various drug and substrate concentrations in the low micromolar range, K_i app was crudely estimated at an upper limit of 5 μM for that subcomponent that was inhibitable. Using lowest possible substrate concentrations, the K_i app for the inhibitable subcomponent was approximated in the low micromolar range, which is far above therapeutic concentrations of free drug.

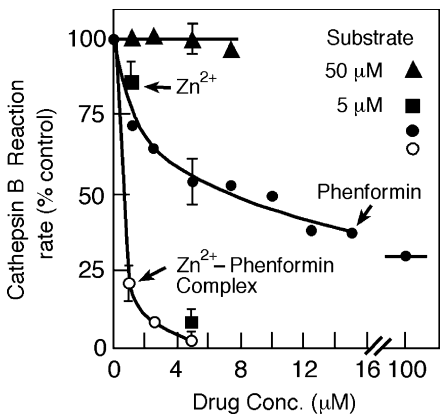

Fig. 4. Inhibition of cathepsin B activity toward Z-Phe-Arg-AMC with Zn^{2+}, phenformin, and the Zn^{2+}–phenformin complex. Measurements represent initial reaction rates of cathepsin B activity toward Z-Phe-Arg-AMC substrate as illustrated in Fig. 5. At substrate concentration of 5 uM, the phenformin concentration causing 50% protease inhibition was approximately 6–7 uM. However, the maximal inhibition caused by phenformin under this substrate concentration was 70%, even at high 100 uM phenformin concentration. At 10-fold higher substrate concentration of 50 uM, phenformin (0–8 uM) did not cause appreciable inhibition of cathepsin B activity, indicating competitive inhibition caused by phenformin alone (triangles). Additional features are described in the text.

In the absence of metal ions metformin did not appreciably inhibit cathepsin B activity toward Z-Phe-Arg-AMC under comparable conditions. However, cathepsin B also hydrolyzes the Z-Arg-Arg-AMC substrate [36]. Therapeutic metformin concentration was found to be a weak competitive inhibitor of cathepsin B activity toward the Z-Arg-Arg-AMC substrate in the absence of metal ions (data not shown). These results caution that a single substrate cannot reveal all inhibitory drug–peptide interactions, nor simulate *in vivo* degradation of the substrate multitude as is possible with the intracellular bioassay. The protease inhibitory actions of proguanil and buformin were not determined.

3.3. Metal-interactive inhibition of cysteine proteases with biguanide drugs

Customary enzyme kinetics could not be applied to biguanide–metal-interactive protease inhibitions; however, the general phenomenon could be readily demonstrated at therapeutic drug levels. Simultaneous interactions among participants include: interactions of drug substituents with protease subsites, independent interactions of metal with the protease catalytic pair, and combined interactions of the drug–metal complex with protease subsites and catalytic pair. In addition, the required DTT of the assay is a metal buffer competing with other binding interactions. The binding kinetics of various metals at the catalytic pair of cysteine proteases is known to be largely noncompetitive with substrate binding to distinct subsites. However, metal inhibition is reactivatable upon metal chelation. Under present assay conditions, the inhibitory actions of 0.5, 1.0, and 5 uM Zn^{2+} alone were 5–10, 10–20, and 95–100% (Fig. 4, and data not shown).

Inhibitory synergy among biguanides and metal ions was observed near the minimally effective inhibitory concentration of metal ions alone. At 1 uM, the Zn^{2+}–phenformin complex caused approximately 80% inhibition, which is more than the additive 25% inhibition caused by 1 uM phenformin and the 15–20% inhibition caused by 1 uM Zn^{2+} under identical conditions (Fig. 4). At higher concentrations of drug and metal, their combined actions were approximately additive in the range of 25–50% inhibitions caused by the independent agents (data not shown). Cathepsin B was completely inhibited by less than 5 uM concentration of the Zn^{2+}–phenformin complex. Thus, phenformin–metal complexation eliminated the 30% subcomponent of reaction that was uninhibited by 100-fold higher concentration of metal-free phenformin alone. These results indicate that metal complexation converts the drug action from a weak, partial competitive inhibitor to a complete inhibitor with much greater potency.

Metals converted metformin from a noninhibitor of cathepsin B or falcipain activity at therapeutic concentrations, to an inhibitory participant (Fig. 5, Table 1). With Z-Phe-Arg-AMC as substrate, metformin (0.5–5 uM) alone had negligible inhibitory action against cathepsin B. Cathepsin B was inhibited 5–10% by 0.5 uM Zn^{2+}; however, 0.5 uM concentration of the Zn^{2+}–metformin complex caused approximately 76% inhibition (Fig. 5). Following inhibitory action of the Zn^{2+}–metformin complex, addition of excess 500 uM EDTA chelator caused complete reactivation of cathepsin B.

Fe^{3+} alone (20 uM) caused 24% inhibition of falcipain activity (Table 1). Whereas 20 uM metformin alone caused

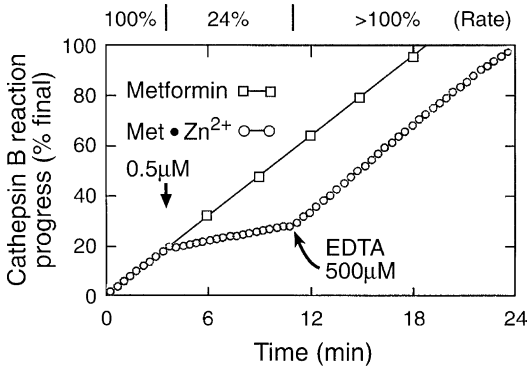

Fig. 5. Inhibition of cathepsin B activity by the Zn^{2+}–metformin complex, and reversal by EDTA. The ongoing control rate of cathepsin B hydrolysis of Z-Phe-Arg-AMC from 0 to 4 min, was statistically extrapolated (continuous trace, $R > 0.96$). Either metformin alone (0.5 uM, squares), or the Zn^{2+}–metformin complex (0.5 uM, open circles) was added at 4 min. In the absence of Zn^{2+}, metformin did not inhibit the reaction as shown at 0.5 uM (squares) or at higher 5 uM concentrations (data not shown). The inhibitory action of 0.5 uM Zn^{2+} alone was approximately 5–10% (data not shown). The Zn^{2+}–metformin complex decreased the slope of the reaction progress to 24% of control reaction rate. Addition of 500 uM EDTA reversed the inhibition caused by the biguanide–metal complex. The slight deceleration in reaction following 18 min is attributable to substrate depletion. Results are representative of three separate determinations.

Table 1
Inhibitory actions of metformin, ferric ion, and the metformin–ferric ion complexes on falcipain-2 activity toward Z-Phe-Arg-AMC substrate

Agent	Percent control activity remaining (±SD, N = 5)
Metformin (20 uM)	100 ± 3.8
Fe^{3+} (20 uM)	76.4 ± 2.4
Fe^{3+}–metformin complex (20 uM)	20.2 ± 1.6
Fe^{3+}–metformin complex (40 uM)	10.6 ± 1.8

no falcipain inhibition, 20 uM Fe^{3+}–metformin complex caused 80% inhibition, which was greater than the sum of independent inhibitions caused by these individual agents separately. At higher 40 uM concentration, the Fe^{3+}–metformin complex caused 90% inhibition of falcipain activity (Table 1). The results of Table 1 were similar with cathepsin B (data not shown). The Fe^{2+} ion was a much less potent inhibitor of both cathepsin B and falcipain than the Fe^{3+} ion. The Fe^{2+} ion alone caused no inhibition of either protease at 20 uM and approximately 25% inhibition at 150 uM (data not shown). The interaction of Fe^{2+} with metformin was weak or absent at therapeutic drug concentration of 20 uM; however, biguanide interactions with Fe^{2+}, or Cu^{2+}, ions were not rigorously characterized. Thus, therapeutic metformin is expected to be interactive with Fe most potently under pro-oxidative intra-erythrocytic conditions (see Section 4).

3.4. Metal-interactive action of biguanide drugs on intracellular proteolytic pathways in primary tissue bioassay

Total cell protein degradation can be experimentally partitioned into distinct major subcomponents using agents of known actions [31–33]. Cell culture is infeasible for present purposes; however, major subcomponents observed in this primary tissue bioassay can be qualitatively defined in quiescent 3T3 cells [32]. The lysosomal pathway is a major route of both mammalian tissue insulin degradation, and parasite hemoglobin degradation, although extravesicular proteolysis might be appreciable.

Immediately following biosynthetic labeling, radiolabeled leucine is released overwhelmingly from the rapidly degraded subcomponent (see Ref. [32]). Rapid turnover proteolysis was eliminated by a preliminary 3-hr degradation period prior to observations. From 3 to 6 hr postlabeling, three stable subcomponents of [^{3}H]leucine release can be readily distinguished (Fig. 6A and B). In this preparation, exposure to experimental agents is initiated by infusion from 100- to 1000-fold concentrated solutions into nonrecirculating perfusate immediately above the organ. Accordingly, the independent effects of two agents can be compared to sequential, concurrent exposure to both, e.g., chloroquine and diamide (Fig. 6A). Chloroquine maximally inhibits 45–48% of total [^{3}H]leucine release, consisting of nearly all of the lysosomal subcomponent. The

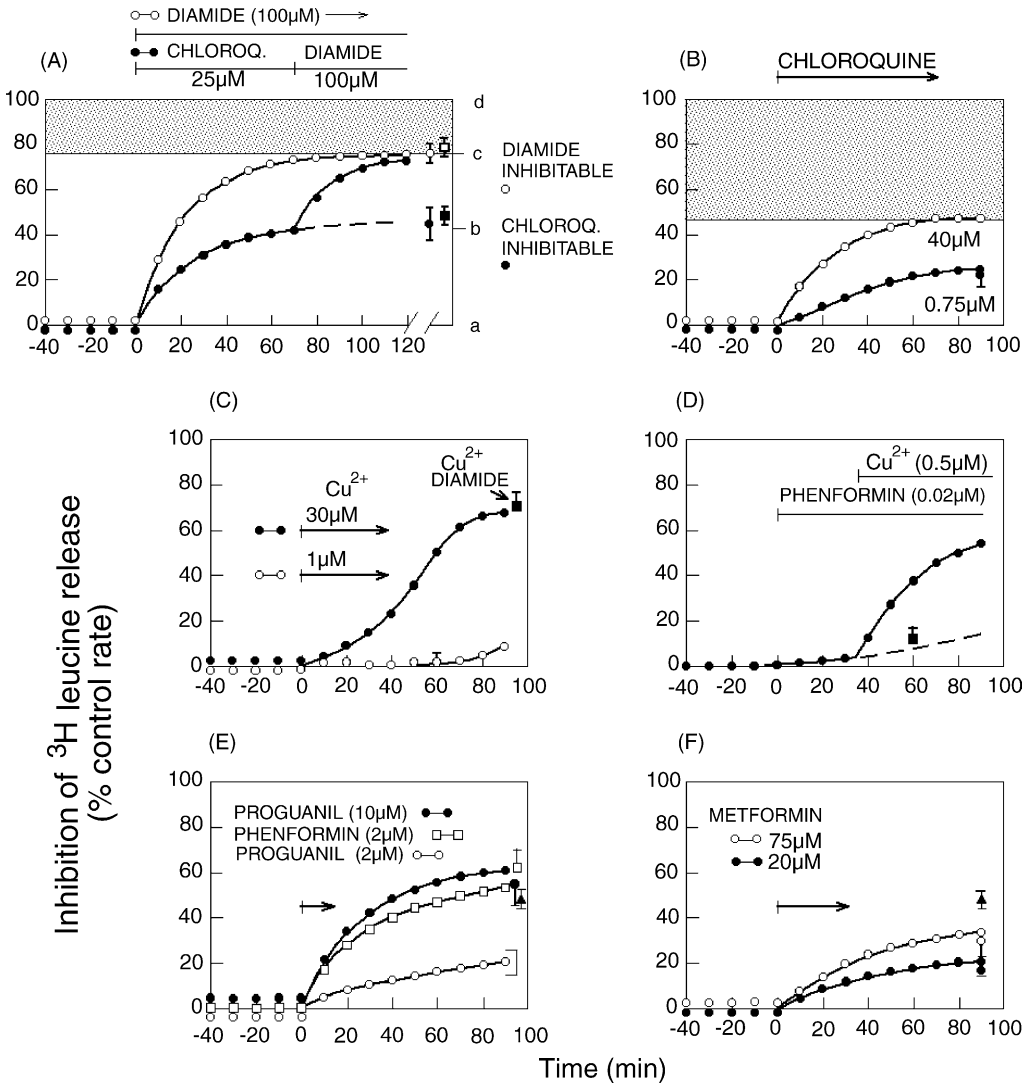

Fig. 6. Pharmacologic inhibitions of intracellular proteolytic pathways using the contractile perfused myocardium as bioassay. Release of [^{3}H]leucine from biosynthetically labeled proteins was determined in nonrecirculating effluent perfusate (see Section 2). Rapid turnover proteolysis was eliminated by a 3-hr preliminary degradation period prior to zero time. The baseline from −40 to 0 time was normalized to 100% control. Each point shown at 10 min intervals represents the statistically fitted trace derived from five measurements at 2 min intervals. Values shown ±SD are means of at least three separate hearts. (A) Individual effects of diamide and chloroquine, and effects of sequentially combined diamide and chloroquine on proteolysis. The unshaded region (a–c) represents the 75% of proteolysis that is diamide-inhibitable, or redox-responsive. The shaded region (c–d) corresponds to the 25% subcomponent that is diamide-uninhibitable or redox-unresponsive. The experiments illustrated in panel A employed 0.1 mM physiologic leucine. The identical experiments with chloroquine (filled square) and diamide (open square) were also performed with supraphysiologic 1 mM leucine in order to detect any possible artifact due to leucine concentration (see Section 2). Under these conditions there was no significant difference among physiologic (0.1 mM) and supraphysiologic (1 mM) leucine ($P > 0.1$, two-sided Student's t-test). Experiments (B)–(F) employed 0.4 mM leucine chase. (B) Effects of therapeutic and supratherapeutic chloroquine concentrations on proteolysis. The shaded region (shown as b–d in panel A) represents the 50–55% of proteolysis that is the chloroquine-resistant or extralysosomal subcomponent. The unshaded region (shown as a–b in panel A) represents the 45–50% chloroquine-inhibitable or lysosomal vesicular proteolysis. Subtraction of the lysosomal subcomponent from the diamide-inhibitable subcomponent defines the extralysosomal redox-responsive subcomponent (b–c in panel A). (C) Effects of 1 and 30 uM Cu^{2+} infusions on proteolysis. Infusion of 30 uM Cu^{2+} caused marked contractile dysfunction. As characterized by the procedure of panel A, combined diamide (100 uM) and Cu^{2+} (30 uM) did not cause inhibition significantly greater than the maximal 75% inhibition caused by either alone ($P > 0.0.1$). (D) Synergistic inhibition of proteolysis caused by exposure to submaximal phenformin followed by concurrent Cu^{2+}. Exposure to submaximal phenformin (0.02 uM), followed by concurrent Cu^{2+} (0.5 uM) caused a marked synergy corresponding to the maximal action of much greater Cu^{2+} concentration (see panel C). The indicated experiment is closely representative of two under these conditions, and similar results using 1 uM Cu^{2+}, or 1 uM Zn^{2+} (data not shown). (E) Effects of near-therapeutic and supratherapeutic proguanil, and supratherapeutic phenformin on proteolysis. The effect of 2 uM proguanil is shown as the mean of two close determinations with range indicated by the bracket. The combined actions of 2 uM proguanil and 25 uM chloroquine (triangle) did not exceed the actions of chloroquine alone (shown statistically in panel A, $P > 0.1$). The 55–60% inhibitory action of supratherapeutic proguanil (10 uM) did significantly include a fraction of extravesicular proteolysis slightly beyond the 45% effect of chloroquine alone ($P < 0.01$), as did supratherapeutic phenformin (20 uM) (data not shown, see text). (F) Effects of therapeutic and supratherapeutic metformin concentrations on proteolysis. The additive actions of combined 75 uM metformin and 25 uM chloroquine (triangle) did not significantly exceed the actions of chloroquine alone (shown in panel B) ($P > 0.0.1$).

gentle reversible sulfhyryl oxidant, diamide, maximally inhibits 75% of proteolysis. Diamide action defines the redox-responsive subcomponent of total cell proteolysis. Combined diamide and chloroquine exposure does not cause additive inhibition greater than the action of diamide alone; therefore the 45–50% lysosomal subcomponent is included in the 75% diamide inhibition. A major subcomponent of 25% of total proteolysis is uninhibited by combined diamide and chloroquine, and is thereby defined as extravesicular, redox-unresponsive proteolysis. An extravesicular, redox-responsive subcomponent is experimentally defined by subtraction of the 45% inhibition caused by chloroquine from the 75% inhibition caused by diamide, yielding 30% of total proteolysis (Fig. 6A and B).

3.4.1. Chloroquine-mimetic actions of biguanide drugs at therapeutic concentrations

The extent of chloroquine antilysosomal action in primary tissue is unknown at therapeutic concentration of approximately 0.75 uM. If chloroquine and biguanide antiproteolytic mechanisms involve distinct actions against the vacuolar transporter and protease active sites, then these convergent mechanisms should both occur at therapeutic drug concentrations.

Therapeutic chloroquine concentration (0.75 uM) did indeed cause an appreciable, but submaximal, inhibition of lysosomal proteolysis. However, full attainment of this submaximal action required approximately 1 hr. Therapeutic chloroquine (0.75 uM) caused 15–20% inhibition of total cell protein degradation, consisting of 30–40% inhibition of the lysosomal subcomponent. Complete inhibition of lysosomal function could be produced by supratherapeutic concentrations of several μM chloroquine as previously described [32].

The antilysosomal action of therapeutic metformin was similar to therapeutic chloroquine despite the two very different initial mechanisms. Therapeutic metformin concentration of 20 uM caused approximately 15–20% inhibition of total proteolysis, consisting of approximately 50% inhibition of the lysosomal subcomponent (Fig. 6F). Simultaneous infusions of supramaximally effective chloroquine (25 uM) and metformin (20 uM) did not cause additive inhibition beyond the maximal effect of chloroquine alone (Fig. 6F). Thus, metformin and chloroquine similarly cause submaximal antilysosomal actions at therapeutic concentrations. Metformin did not cause full inhibition of the lysosomal subcomponent even at supratherapeutic 100 uM concentration, which caused 80% lysosomal inhibition. The submaximal actions of metformin appeared stable over the feasible observation period of 1.5–2.0 hr. Phenformin is submaximally antiproteolytic at only 0.02–0.20 uM which is well within its therapeutic concentration (Fig. 6D). Surprisingly, phenformin caused maximal lysosomal inhibition at slightly supratherapeutic concentration of only 2 uM (Fig. 6E).

At therapeutic concentrations, proguanil (2 uM) similarly inhibited 15–25% of total proteolysis, corresponding to 30–50% of the lysosomal pathway (Fig. 6E). The major uncertainty of this bioassay is the possibility of progressive proteolytic inhibition delayed beyond the maximal possible observation period of approximately 2 hr exposure. When 10-fold supratherapeutic proguanil or phenformin (10 uM) were infused, the lysosomal pathway was first inhibited (Fig. 6E). However, prolonged infusion of supraphysiologic proguanil or phenformin (10 uM) secondarily caused a gradual inhibition of some extralysosomal proteolysis, e.g., 55–60% inhibition of total proteolysis over 2 hr (data not shown). The significance of such high drug concentrations is unknown; however, no apparent contractile dysfunction accompanied these proteolytic inhibitions. Thus, the lysosomal pathway is undoubtedly most sensitive to biguanides over present observation periods. Whether prolonged exposures to therapeutic proguanil or phenformin secondarily cause partial inhibitions of extralysosomal proteolysis is unknown.

3.4.2. Inhibitory effects of extracellular metal ion exposures on bioassayed intracellular proteolytic pathways

Exchangeable serum Zn^{2+} and Cu^{2+} concentrations are several μM [42,43]. This perfusate contains excess amino acids and citrate, which are the major extracellular metal buffers. Present objectives do not require exact simulation of endogenous free metal concentrations or transport.

Infusion of 1 uM Zn^{2+} or Cu^{2+} caused little change in protein degradation over nearly 1 hr (Fig. 6C, and data not shown). After a lag time of approximately 1 hr, micromolar metal exposure caused a gradually increasing partial proteolytic inhibition over the following 1–2 hr. Continuous infusion of supraphysiologic 30 uM Zn^{2+} or Cu^{2+} caused inhibitions of nearly all diamide-sensitive proteolysis by 1 hr of exposure (Fig 6C). These high 30 uM metal concentrations also caused contractile abnormalities after 1 hr, indicating nonphysiologic metal accumulations and/or distributions. Simultaneous exposure to diamide and supraphysiologic metals nonadditively inhibited the same 75% of total proteolysis. Although not rigorously characterized, minimally effective concentrations of metals inhibited the chloroquine-sensitive, lysosomal pathway selectively over a 1 hr exposure.

3.4.3. Synergistic antiproteolytic actions of extracellular biguanide drugs and metal ion

Simultaneous co-infusion of metals and biguanides results in rapid formation of biguanide–metal complexes in the extracellular perfusate, and permeated intracellular compartments [1]. Following the submaximal action of minimal phenformin (0.02 uM) alone, the simultaneous infusion of inactive Cu^{2+} concentration (0.5 uM) caused a marked synergy in the potency, time course, and maximal antiproteolytic action of phenformin (Fig. 6C and D). The

Cu^{2+}–phenformin complex at only 0.02 uM gradually inhibited both lysosomal and extravesicular proteolysis consisting of the entire 75% diamide-sensitive subcomponent. This combined infusion of phenformin and Cu^{2+} caused pathogenic compromise in contractile function at 60 min, indicating nonphysiologic conditions. This remarkable 75% proteolytic inhibition caused by supraphysiologic metal loading probably exceeds maximal fluctuations in steady state protein turnover *in vivo*. In two experiments each, infusion of the Cu^{2+} or Zn^{2+} complexes of metformin (2 uM) inhibited all of the lysosomal pathway in 1 hr, beginning immediately (data not shown). Thus, upon infusion of the nonbound drug (Fig. 6F), the acquired distribution of endogenous inhibitory metal ions differs from the retained metals of the preformed complex under this method of experimental delivery (see Section 4). The Fe^{3+}–biguanide complexes were not similarly characterized.

3.5. Models of ligand interactions between the metal complex of phenformin and the active site of cathepsin B

The docking program employs a three-dimensional enzyme structure, and separately computed ligand structure in order to compute and display feasible binding orientations. Binding alignments are computed by comparison of the shape and charge complementarity of protein-binding sites and hypothetical ligands tested. Multiple binding orientations are common among protein ligands [41]. Interpretation and limitations of dock modeling have been critically reviewed [37,38].

Among various inhibitory metals bound by biguanides, the Fe^{3+} complex was employed for initial modeling in view of its relevance to intra-erythrocytic parasite growth under oxidative stress (see Section 4). Overall protease–ligand alignment represents a compromise between the attractions of the drug substituent group for subsites vs. shared drug–protease metal attractions at the catalytic pair. As predicted from substrate–drug structural homologies, a major phenformin-binding mode involves phenyl binding at the protease S2 pocket, and shared metal co-binding at the protease catalytic pair (Fig. 3C and D). The drug phenyl group alignment is strikingly homologous to the well-known S2–P2 interaction of the Phe-Arg substrate motif. Docking programs provide *in vacuo* computation of the total decrease in free energy upon binding in a particular orientation. The major binding mode illustrated is associated with a large total binding energy exceeding −100 kcal/mol.

The surfaces of most proteins include random constellations of amino acids with hydrophobic binding properties, i.e., ''greasy spots'', or metal-attractive properties that are relevant to the binding of a phenyl-containing metal complex. As expected, the surface of cathepsin B exhibited weak binding of the Fe^{3+}–phenformin complex at locations outside the active site (not shown).

Vicinal structures surrounding the catalytic amino acids can indirectly influence enzyme reaction mechanisms and/or metal binding. The negative character of carbonyl oxygens of the peptide backbone are known to interact with some enzyme reaction mechanisms if located at short distance. In human cathepsin B the position of the carbonyl oxygen of the peptide backbone at Gly198 is in close proximity to the catalytic amino acid pair. Although beyond the present scope, the carbonyl oxygen of Gly198 is believed to exert a subtle, interactive effect on the reaction mechanism of cathepsin B [36,39]. These three known metal-attractive sites comprise a triangle with side distances between atomic centers of: Cys-His = 3.81 Å, Cys-Gly = 4.89 Å, His-Gly = 4.7 Å (Fig. 3B and C). Charge attractions are presumed to be operative in docking at distances appreciably less than 2 Å. Thus, the triangle bounded by the inter-atomic distances of these three metal-attractive sites is consistent with known features of a metal cation-binding triad. The shared drug-bound metal is computed in an alignment above the plane of the triangle represented by the dashed traces in Fig. 3B. Other carbonyl oxygens do not appear sufficiently close to contribute appreciably to the metal coordination illustrated in Fig. 3B as shown by the carbonyl oxygen of His199 below the plane of the triangle in views A and B. Sufficient metal concentrations can inhibit the Cys-His pair of all cysteine proteases, including those without the exact Gly198 carbonyl conformation of cathepsin B [36,39]. However, the proximity of this Gly198 carbonyl oxygen of cathepsin B appears to contribute additional negative charge attraction to metal cation binding shared between the Cys29-His199.

Computations revealed multiple, feasible binding modes, consistent with known features of protease–ligand interactions. The locations of distinct subsites known as S1 and S2′ have been described in Ref. [36] (not shown here). In contrast to the S2 site, these other subsites are not recessed pockets but rather surface regions that are believed to contribute to some substrate attractions. The shared drug–metal anchor at the catalytic pair also permits the phenyl group of the Fe^{3+}–phenformin complex to align with the S1 subsite (left of catalytic pair in Fig. 3), and S2′ subsite (right of catalytic pair). However, the computed binding energies of the S1 and S2′ alignments are less than that of the S2 alignment, indicating that both are lesser binding modes (data not shown). Less favored phenyl binding at the S1 subsite aligns the metal at a displacement from that shown near the center of the binding triad because the S1 subsite is closer to the catalytic pair than the S2 subsite (not shown). Multi-modal drug binding might explain multi-modal inhibition toward a single substrate (Fig. 4), or versatile inhibitions toward the endogenous substrate multitude.

The dimethyl substituents of metformin bear only partial homology to the phenyl group of phenformin. The attraction of the S2 pocket for the phenformin phenyl group

presumably imparts greater subsite binding tendency than metformin, thereby explaining the contrasting inhibitory actions of the noncomplexed drugs toward Z-Phe-Arg-AMC as described above. The Fe^{3+}–metformin complex docked in several binding modes with the metal ion shared almost equidistant between the three metal-attractive groups; however, docking of metformin and proguanil have been only qualitatively verified thus far (data not shown).

4. Discussion

4.1. Intracellular metal ion homeostasis and metal-interactive inhibition of lysosomal proteases with biguanide drugs

Metals alone can inhibit cysteine protease reactions; and supraphysiologic metal loading can inhibit most of cell protein degradation. In addition to protease–metal co-binding, drug–metal complexation might subvert unknown endogenous mechanisms protecting protease reactions against inhibitory metals. Beyond the present scope, metal ion regulation involves transport, intracellular compartmentation, sequestration by tight binding, partition among lower affinity buffers, and redox regulation of metals and/or metal-binding sites [42,43]. Metal homeostasis differs markedly among tissues. Biguanides might remove metals from buffering sites, shield ion charge, introduce hydrophobicity, and/or chemical reactivities, decrease removal of metal from protease by unknown mechanisms, increase membrane permeability, interfere with metal transport or compartmentation, and increase protease associative properties. Drug enhancement of metal binding might secondarily catalyze sulfur oxygenations as well as direct protease inactivation.

Following protease binding of the biguanide–metal complex, the biguanide could dissociate, leaving the inhibitory metal bound to the catalytic pair. A transcompartmental metal shuttle might explain the remarkable effectiveness, and toxicity of the Cu^{2+}–phenformin complex under constant experimental delivery at low concentration. Oral or parenteral administration of a preformed biguanide–metal complex would cause disequilibrium exposure to that complex if the metal exchange time is slower than the time of distribution, permeation, and action. Future investigations might discover potent antiproteolytic actions among some preformed biguanide complexes with biologic or nonbiologic metals [44].

4.2. Iron-interactive biguanide antiproteolytic action in malaria therapy

Cure, subcurative control, or prophylaxis need not kill parasites, but rather slow their growth to a rate that can be overcome or balanced by host immunity. In general, the parasite sensitivity to nonspecific proteolytic inhibition exceeds that of the host, thereby providing an exploitable therapeutic advantage. Parasite growth can be limited by obligate hemoglobin degradation [24,25], and other functions of parasite proteolysis. Plasmodial hemoglobin degradation involves multiple types of proteases in a sequence of events that can be retarded by nonspecific cysteine protease inhibitors [23]. Protease inhibitors need not be completely specific for target parasite proteases in order to effectively inhibit *in vivo* parasite growth [24]. Indeed, chloroquine treats malaria by nonspecific interference with the vacuolar transporter of both parasite and host tissues.

Nonprotein Fe^{3+} from degraded hemoglobin is a natural inhibitor of parasite proteolysis in conjunction with oxidative stress caused in erythrocytes by plasmodia. The metallic and oxidative metabolic environment within infected erythrocytes might confer selective enhancement of biguanide action against plasmodial proteolysis. Although most of the large amount of nonprotein Fe from degraded hemoglobin is in the form of heme, a small fraction of nonheme Fe would suffice to occupy 20 uM therapeutic biguanide. Proguanil is routinely administered in combination with pro-oxidative drugs that cause 5–10% Fe^{2+} oxidation to Fe^{3+}. Therefore, even low subcurative doses of pro-oxidative drugs would be expected to produce sufficient oxidized nonprotein Fe^{3+} to saturate therapeutic biguanide concentration. Indeed, extracellular Fe, Cu, and Zn could provide complete occupancy and activation of 20 uM biguanide or more.

Preliminary results indicate that growth of *P. falciparum* in erythrocyte culture is 50% inhibited by 60 uM metformin. This metformin potency has not yet been investigated in the presence of presumably synergistic pro-oxidative drugs and Fe^{2+} oxidation. In the presence of host immunity and pro-oxidant drugs, the antimalarial effect of metformin might be appreciable at tolerable concentrations without cross-resistance to chloroquine. Regardless, proguanil and metformin are two drugs that exhibit antihyperglycemic, antimalarial, and antiproteolytic actions.

4.3. Zinc-interactive biguanide antiproteolytic action in anti (type 2) diabetic therapy

Evidence is accumulating in support of the old hypothesis of insulin hypercatabolism among multiple causes of insulin insensitivity [7–20]. (1) In animal models chloroquine decreases insulin degradation, and prolongs its action [7,8]. (2) In clinical trials chloroquine enhances multiple insulin actions including both carbohydrate and lipid metabolism [11,15–17]. (3) Either chlororoquine or metformin markedly decrease the ongoing exogenous insulin requirement in type 2 diabetic individuals by 30–40% [9,10,12]. Indeed, failure to decrease ongoing insulin dosage prior to initiation of chloroquine can result in life-threatening hypoglycemia [18]. (4) In the absence of

exogenous insulin, chloroquine overdose has caused hypoglycemia in some nondiabetic individuals [15,20,45]. (5) Force-feeding rats causes insulin hypercatabolism and insulin resistance, which can be reversed by chloroquine [14]. (6) A recent study of unrelated hypotheses is consistent with radiolabeled insulin hypercatabolism in type 2 diabetic forearm muscles, and reversal with metformin [19]. (7) Many studies show that Tumor Necrosis Factor (TNF) alpha can cause insulin resistance of unknown significance [30]. Supraphysiologic TNF can also cause muscle wasting syndrome (cachexia), and death by liver apoptosis [29]. In knockout mice the absence of cathepsin B results in a dramatic decrease in the hepatic destruction and death caused by TNF, although the linking mechanism is not yet known [29]. Implications are that TNF might somehow contribute to insulin resistance by unexplained activation of cathepsin B and insulin degradation. Insulin hypercatabolism is not inconsistent with diabetic hyperinsulinemia under compensatory elevation in release [13].

The surface of insulin contains an unusually large number of Zn^{2+}-binding sites. Zn^{2+} alone is a potent and effective natural inhibitor of many proteases. It has long been suspected that insulin-bound Zn^{2+} serves as a natural shield against protease attack within the protease substrate microenvironment. The excess of biguanide could directly co-bind Zn^{2+} ions on the surface of insulin, thereby concentrating metformin in the protease-substrate microenvironment. Diabetic abnormalities in zinc status have been repeatedly reported; however, the relevance to present studies remains unknown [46].

4.4. Contrary to hypothesis

It is conceivable that the reported antimitochondrial action of biguanides [3–6] is somehow linked to an unknown antilysosomal effect common to both malaria and diabetic therapy. Such indirect, metabolic antiproteolytic actions would not negate the hypothesis of direct protease active site inhibition, i.e., multiple antiproteolytic actions. Moreover, the antiproteolytic hypothesis is not inconsistent with additional nonproteolytic drug mechanisms.

4.5. Therapeutic feasibility of lifetime cysteine protease inhibition as revealed by biguanide retrospective

Knockout of cathepsin B alone is dispensable with little adverse effect on mice [47]. However, combined knockout of multiple cysteine proteases causes interesting lethal neuropathogenesis 2 months postnatal [47]. Maximal, nonspecific cysteine protease inhibition might eventually cause a neuropathic failure of catabolism syndrome, similar to multiple protease knockouts [47,48].

Most discovery programs seek maximally effective drugs that tightly bind to target proteases with high specificity, sparing nontarget proteases. In contrast, the safe antiproteolytic actions of therapeutic biguanides are: (a) nonspecific for particular cysteine proteases, inhibiting both B and L cathepsins (b) submaximally effective at therapeutic concentrations, and (c) dependent upon endogenous metal microenvironment as well as the subsite-binding properties of the drug. Efficacy and safety might not be optimized by completely specific or maximally effective prolonged protease inhibition. Both insulin and intraparasitic hemoglobin are degraded by multiple cysteine proteases and other proteases [23,25]. Inhibition of one cysteine protease does not eliminate alternative, redundant degradative pathways. It is possible that chloroquine is a tolerable and effective antimalarial/antidiabetic drug due to nonselective, *partial* inhibition of lysosomal proteolysis. However, future biguanides with selective, maximal protease inhibitory actions might serve some short-term applications, e.g., radical cure of parasitic infections [24].

Despite unpredictable toxicity, chloroquine has been used in therapy of more than 30 diseases, presumably served by antilysosomal actions [20,22,45]. Much pathogenesis from chloroquine overdose is the direct result of vacuolar-degradative inhibition. Following chloroquine overdose, electron microscopy of myocardial biopsies reveals swollen lysosomes accompanied by undegraded macromolecular cytoplasmic debris from ruptured vesicles. The primary tissue bioassay suggests that safe chloroquine or biguanide exposures involve submaximal inhibition of less than half of lysosomal function. Biguanides are converging, chloroquine-mimetic, antiproteolytic agents with different initial mechanism and lesser side effects. Biguanides do not cause pathogenic vesicular swelling and rupture, and presumably do not inhibit the vacuolar transporter. Past metformin administration suggests that submaximal, nonspecific cysteine protease inhibitors can be effective in some applications, and safe over lifetime administration [21]. Present or future biguanides might substitute for chloroquine with much less risk, or permit combination therapy with lower chloroquine.

4.6. Employment of guanidyl guanidine as scaffold for synthesis of safe protease inhibitors

In addition to diabetes and malaria, the diverse functions of cathepsins, calpains, caspases, and other proteases suggest many potential applications of nonspecific or preferential biguanide derivatives, e.g., rheumatoid arthritis, lupus [20,45], other inflammation, bone resorption, pancreatitis [49], cachexia, apoptosis [29], and others. Biguanide can serve as a scaffold for synthesis of inestimable numbers of derivatives at both termini using combinatorial chemistry. Recombinant target enzymes can serve as disease surrogates for automated, high throughput inhibitor screening. Using dock modeling, studies in progress are attempting to predict the likely subsite binding and effectiveness of hypothetical biguanide derivatives not yet synthesized.

Acknowledgments

Supported by grants from the Diabetes Foundation of the Hoechst Company, and the National Science Foundation (NSF/CISE-EIA-0122582).

References

[1] Prugnard E, Noel M. Chemistry and structure–activity relationships of biguanides. Handbook Exp Pharmacol 1995;119:263–82.
[2] Slotta KH, Tschesche R. Uber Biguanide. II. Die Blutzucker-senkende Wirking der biguanide. Ber Otch Chem Gessel 1929;62 B:1398–405.
[3] El-Mir MY, Nogueir V, Fontaine E, Averet N, Rigoulet M, Levrve X. Dimethylbiguanide inhibits cell respiration via an indirect effect targeted on the respiratory chain complex I. J Biol Chem 2000; 275:223–8.
[4] Owen MR, Doran E, Halestrap AP. Evidence that metformin exerts its antidiabetic effects through inhibition of complex I of the mitochondrial respiratory chain. Biochem J 2000;348:607–48.
[5] Fidock DA, Wellems TE. Transformation with human dihydrofolate reductase renders malaria parasites insensitive to WR 99210 but does not affect the intrinsic activity of proguanil. Proc Natl Acad Sci USA 1997;94:10931–6.
[6] Fidock DA, Nomura T, Wellems TE. Cycloguanil and its parent compound proguanil demonstrate distinct activities against *Plasmodium falciparum* malaria parasites transformed with human dihydrofolate reductase. Mol Pharmacol 1998;54:1140–7.
[7] Bevan AP, Krook A, Tikerpae J, Seabright PJ, Siddle K, Smith GD. Chloroquine extends the lifetime of the activated insulin receptor complex in endosomes. J Biol Chem 1997;272(26):833–40.
[8] Blazar BR, Whitly CB, Kitabchi AE, Tsai MY, Santiago J, White N, Stentz FB, Brown DM. In vivo chloroquine-induced inhibition of insulin degradation in a diabetic patient with severe insulin resistance. Diabetes 1984;33:1133–7.
[9] Emani J, Gersten HC, Pasutto FM, Janmali F. Insulin-sparing effect of hydroxychloroquine in diabetic rats is concentration dependent. Can J Physiol Pharmacol 1999;77:118–23.
[10] Fritsche A, Schmulling RM, Haring HU, Stumvoll M. Intensive insulin therapy combined with metformin in obese type-2 diabetic patients. Acta Diabetol 2000;37:13–8.
[11] Gerstein HC, Thorpe KE, Taylor DW, Haynes RB. The effectiveness of hydroxychloroquine in patients with type 2 diabetes mellitus who are refractory to sulfonylureas—a randomized trial. Diabetes Res Clin Pract 2002;55:209–19.
[12] Jaber LA, Nowak SN, Slaughter RR. Insulin–metformin combination therapy in obese patients with type-2 diabetes. J Clin Pharmacol 2002;42:89–94.
[13] Kitabchi AE, Stentz FB, Cole C, Duckworth WC. Accelerated insulin degradation: an alternate mechanism for insulin resistance. Diabetes Care 1979;2:414–7.
[14] Li C, Zhang S, Shu C. Effects of chloroquine on insulin sensitivity in insulin-resistant rats. Zhonghua Yi Xue Za Zhi (Natl Med J China) 1999;79:867–9.
[15] Petri M. Hydroxychloroquine use in the Baltimore Lupus Cohort: effects on lipids, glucose and thrombosis. Lupus Suppl 1996;1:S16–22.
[16] Powrie JK, Shojaee-Moradic F, Watts GF, Smith GD, Sonksen PH, Jones RH. Effects of chloroquine on the dyslipidemia of non-insulin dependent diabetes mellitus. Metabolism 1993;42:415–9.
[17] Quatraro A, Consoli G, Magno M, Caretta F, Nardozza A, Ceriello A, Giugliano D. Hydroxychloroquine in decompensated, treatment-refractory noninsulin dependent diabetes mellitus. A new job for an old drug? Ann Intern Med 1990;112:678–81.
[18] Shojana K, Koehler BF, Elliot T. Hypoglycemia induced by hydroxychloroquine in a type 2 diabetic treated for polyarthritis. J Rheumatol 1999;1:195–6.
[19] Valensi P, Behar A, Cohen-Boulakia F, Valensi J, Wiernsperger N, Attali JR. In-vivo kinetics of 123 iodine-labelled insulin in skeletal muscle of patients with type-2 diabetes: effects of metformin. Diabet Metab 2002;28:95–103.
[20] Wallace DJ. The use of chloroquine and hydroxychloroquine for non-infectious diseases other than rheumatoid arthritis or lupus: a critical review. Lupus Supl 1996;1:S59–64.
[21] Howlett HC, Bailey C. A risk-benefit analysis of metformin in type-2 diabetes mellitus. Drug Saf 2001;6:489–503.
[22] Stein M, Bell MJ, Ang LC. Hydroxychloroquine neuromyotoxicity. J Rheumatol 2000;27(2):927–31.
[23] Rosenthal PJ. Hydrolysis of erythrocyte proteins by proteases of malarial parasites. Curr Opin Hematol 2002;2:140–5.
[24] Rosenthal PJ, Lee GK, Smith RE. Inhibition of a *Plasmodium vinckei* cysteine proteinase cures murine malaria. J Clin Invest 1993;91:1052–6.
[25] Sajid M, McKerrow JH. Cysteine proteases of parasitic organisms. Mol Biochem Parasitol 2002;120:1–2.
[26] Shenai BR, Sijwali PS, Singh A, Posenthal PJ. Characterization of native and recombinant falcipain-2, a principle trophozoite cysteine protease and essential hemoglobinase of *Plasmodium falciparum*. J Biol Chem 2000;275:29000–10.
[27] Shenai BR, Rosenthal PJ. Reducing requirements for hemoglobin hydrolysis by *Plasmodium falciparum* cysteine proteases. Mol Biochem Parasitol 2002;122:99–104.
[28] Carlton JM, Fidock DA, Djimde A, Plowe CV, Wellems TE. Conservation of a novel vacuolar transporter in *Plasmodium* species and its central role in chloroquine resistance of *P. falciparum*. Curr Opin Microbiol 2001;4:415–20.
[29] Guicciardi ME, Miyoshi H, Bronk SF, Gores GJ. Cathepsin B knockout mice are resistant to tumor necrosis factor-alpha mediated hepatocyte apoptosis and liver injury: implications for therapeutic applications. Am J Pathol 2001;159:2045–54.
[30] Moller DE. Potential role of TNF-alpha in the pathogenesis of insulin resistance and type-2 diabetes. Trends Endocrinol Metab 2000;11: 212–7.
[31] Lockwood TD. Redox-dependent and redox-independent subcomponents of protein degradation in perfused myocardium. Am J Physiol 1999;276:E945–54.
[32] Lockwood TD. Redox control of protein degradation [review]. Antioxid Redox Signal 2000;2:851–78.
[33] Lockwood TD. Cathepsin B responsiveness to glutathione and lipoic acid redox. Antioxid Redox Signal 2002;4:681–92.
[34] Kirschke H, Barrett AJ, Rawlings ND. Proteinases 1: lysosomal cysteine proteinases. Protein Profile 1995;2:1581–643.
[35] Nagase N, Salvesen GS. Finding, purification and characterization of protease inhibitors. In: Beynon R, Bond JS, editors. Proteolytic enzymes: a practical approach. 2nd ed. Oxford University Press; 2001 [chapter 6].
[36] Musil D, Zucic D, Turk D, Engh RA, Mayr I, Huber R, Popovic T, Turk V, Towatari T, Katanuma N. The refined 2.15 Å X-ray crystal structure of human liver cathepsin B: the structural basis for its specificity. EMBO J 1991;10(2):321–30.
[37] Ritchie DW. Protein docking using spherical polar Fourier correlations. Proteins: Struct Funct Genet 2000;39:178–94.
[38] Halperin I, Ma B, Wolfson H, Nussinov R. Principles of docking: an overview of search algorithms and a guide to scoring functions. Proteins 2002;47:409–43.
[39] Nagler DK, Tam W, Storer AC, Krupa JC, Mort JS, Menard R. Interdependence of sequence and positional specificities for cysteine proteases of the papain family. Biochemistry 1999;38:4868–74.
[40] Turk D, Guncar G, Podobnik M, Turk B. Revised definition of substrate binding sites of papain-like cysteine proteases. Biol Chem 1998;379:137–47.

[41] Ma B, Shatsky M, Wolfson HJ, Nussinov R. Multiple diverse ligands binding at a single protein site: a matter of pre-existing populations. Protein Sci 2002;2:184–97.
[42] Huffman DL, O'Halloran TV. Function, structure and mechanisms of intracellular copper trafficking proteins. Annu Rev Biochem 2001; 70:677–701.
[43] MacDiarrmid CW, Gaither LA, Eide D. Zinc transporters that regulate zinc storage in *Saccharomyces cerevisiae*. EMBO J 2002;19:2845–55.
[44] Woo LC, Yuen VG, Thompson KH, McNeill JH, Orvig C. Vanadyl–biguanide complexes as potential synergistic insulin mimics. J Inorg Biochem 1999;30:251–7.
[45] D'Cruz D. Antimalarial therapy: a panacea for mild lupus? Lupus 2001;10:148–51.
[46] Tallman DL, Taylor CG. Potential interactions of zinc in the neuroendocrine disturbances of diabetes mellitus type-2. Can J Physiol Pharmacol 1999;77:919–33.
[47] Felbor U, Kessler B, Mothes W, Goebel H, Ploegh H, Bronson RT, Olsen BR. Neuronal loss and brain atrophy in mice lacking cathepsins B and L. Proc Natl Acad Sci USA 2002;99:7883–8.
[48] Taylor JP, Hardy J, Fischbeck KH. Toxic proteins in neurodegenerative disease. Science 2002;296:1991–5.
[49] Hallangk W, Lerch MM, Brandt-Nedely BB, Roth W, Ruthenbruerger M, Reinheckel T, Domschke W, Lippert H, Peters C, Deussing J. Role of cathepsin B in intracellular trypsinogen activation and the onset of acute pancreatitis. J Clin Invest 2000;106:773–81.